Splice variant–specific cellular function of the formin INF2 in maintenance of Golgi architecture

Vinay Ramabhadran[a], Farida Korobova[a], Gilbert J. Rahme[b], and Henry N. Higgs[a]
[a]Department of Biochemistry, Dartmouth Medical School, Hanover NH 03755; [b]Norris Cotton Cancer Center, Dartmouth Medical School, Lebanon NH 03766

ABSTRACT **INF2 is a unique formin that can both polymerize and depolymerize actin filaments. Mutations in INF2 cause the kidney disease focal and segmental glomerulosclerosis. INF2 can be expressed as two C-terminal splice variants: CAAX and non-CAAX. The CAAX isoform contains a C-terminal prenyl group and is tightly bound to endoplasmic reticulum (ER). The localization pattern and cellular function of the non-CAAX isoform have not been studied. Here we find that the two isoforms are expressed in a cell type–dependent manner, with CAAX predominant in 3T3 fibroblasts and non-CAAX predominant in U2OS, HeLa, and Jurkat cells. Although INF2-CAAX is ER localized in an actin-independent manner, INF2–non-CAAX localizes in an actin-dependent meshwork pattern distinct from ER. INF2–non-CAAX is loosely attached to this meshwork, being extracted by brief digitonin treatment. Suppression of INF2–non-CAAX causes fragmentation of the Golgi apparatus. This effect is counteracted by treatment with the actin monomer–sequestering drug latrunculin B. We also find discrete patches of actin filaments in the peri-Golgi region, and these patches are reduced upon INF2 suppression. Our results suggest that the non-CAAX isoform of INF2 serves a distinct cellular function from that of the CAAX isoform.**

Monitoring Editor
Rong Li
Stowers Institute

Received: May 27, 2011
Revised: Oct 6, 2011
Accepted: Oct 6, 2011

INTRODUCTION

Formin proteins comprise a class of actin assembly factors that accelerate actin filament nucleation and modulate filament elongation rate (Kovar, 2006; Chesarone *et al.*, 2010). There are 15 mammalian formins, which can be classified into seven different phylogenetic groups (Higgs and Peterson, 2005). A key feature of all formins is the presence of the formin homology 1 (FH1) and formin homology 2 (FH2) domains, which are necessary for actin nucleation acceleration and subsequent regulation of barbed-end elongation (Kovar and Pollard, 2004; Higgs, 2005). A subset of formins, termed Diaphanous-related formins (Drfs), are postulated to be regulated by an autoinhibitory interaction between an N-terminal Diaphanous inhibitory domain (DID) and a C-terminal Diaphanous autoregulatory domain (DAD). For at least some Drfs, Rho GTPases relieve this autoinhibition by binding a region overlapping the DID. Recent studies have implicated formins as playing a key role in many cellular functions, including intracellular transport, cytokinesis, and cell migration (Campellone and Welch, 2010).

INF2 is a unique Drf formin that can accelerate both actin polymerization and depolymerization (Chhabra and Higgs, 2006). INF2's depolymerization activity depends on the DAD, which also acts as a WH2-like actin monomer–binding motif. Despite possessing both DID and DAD, INF2 appears to have altered regulatory properties, since DID is ineffective at inhibiting actin polymerization (Chhabra *et al.*, 2009). INF2 is particularly interesting in view of its role in the kidney disease focal and segmental glomerulosclerosis (FSGS). Mutations in the DID of INF2 strongly correlate with FSGS in a number of families (12–17%) afflicted with this disease (Brown *et al.*, 2010; Boyer *et al.*, 2011; Gbadegesin *et al.*, 2011; Lee *et al.*, 2011). The cells affected in FSGS are podocytes—epithelial cells in the glomerulus—whose actin-rich foot processes are vital for appropriate glomerular filtration (Faul *et al.*, 2007).

Despite the clear correlation between INF2 and FSGS, the cellular role of INF2 is incompletely understood. In Swiss 3T3 fibroblasts, INF2 is tightly bound to endoplasmic reticulum (ER), an interaction that depends upon its C-terminal prenylation (Chhabra *et al.*,

This article was published online ahead of print in MBoC in Press (http://www.molbiolcell.org/cgi/doi/10.1091/mbc.E11-05-0457) on October 12, 2011.

Address correspondence to: Henry N. Higgs (henry.higgs@dartmouth.edu).

Abbreviations used: DAD, diaphanous autoregulatory domain; DID, diaphanous inhibitory domain; Drf, diaphanous-related formin; ER, endoplasmic reticulum; FH1, formin homology 1; FH2, formin homology 2; FSGS, focal and segmental glomerulosclerosis; HSP, high-speed pellet; HSS, high-speed supernatant; latB, latrunculin B; LSP, low-speed pellet; LSS, low-speed supernatant; TRITC, tetramethylrhodamine isothiocyanate.

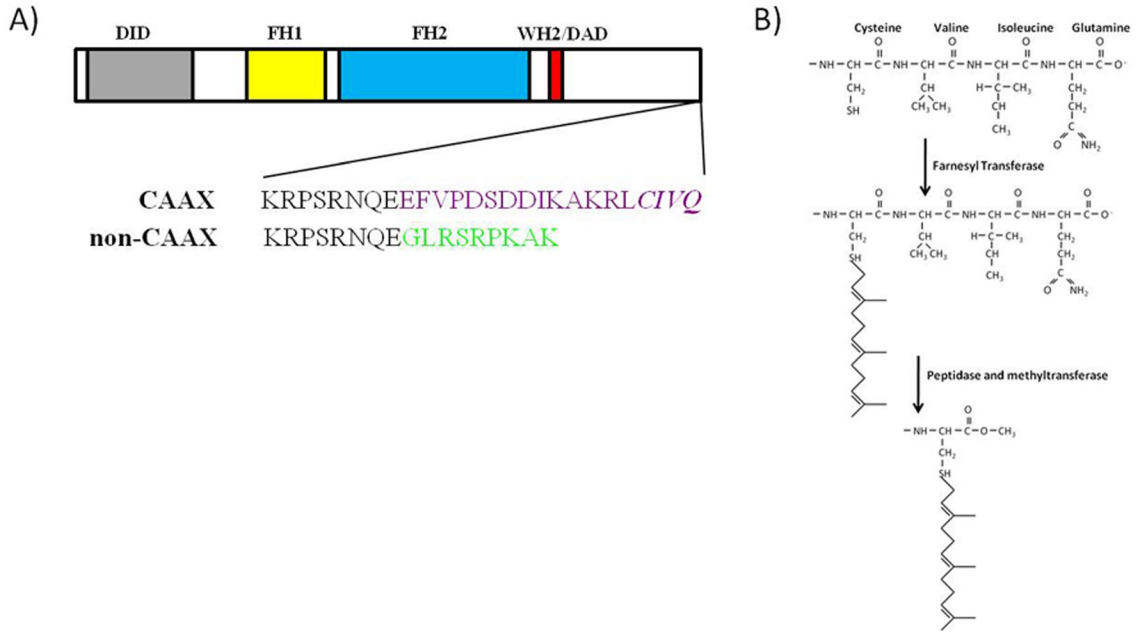

FIGURE 1: INF2 splice variants. (A) Domain architecture of INF2. C-Terminal sequences starting at K1224 of human INF2. The CAAX and non-CAAX splice variants are shown in purple and green amino acids, respectively. (B) Schematic of posttranslational modifications associated with prenylation.

2009). Suppression of INF2 expression does not noticeably alter ER morphology, but overexpression of an INF2 DAD/WH2 mutant causes massive ER-associated actin polymerization and ER collapse (Chhabra *et al.*, 2009).

Recently there have been interesting reports on the cellular roles of INF2. Alonso and colleagues have shown that INF2 interacts with MAL proteins—integral membrane proteins that reside on Golgi and endosomal membranes (Puertollano and Alonso, 1999; de Marco *et al.* 2002). In hepatocyte-derived HepG2 cells, INF2 knockdown inhibits MAL2-dependent transcytosis (Madrid *et al.*, 2010). In Jurkat leukemic T cells, INF2 knockdown inhibits MAL-dependent post-Golgi trafficking of Lck to the plasma membrane (Andres-Delgado *et al.*, 2010). These functions are inconsistent with INF2 localization to ER, raising questions about the role of INF2 in these processes.

One possibility is that splice variants of INF2 have distinct cellular functions. INF2 has two C-terminal splice variants: the CAAX variant, with its C-terminal prenylation site that is critical for stable ER association (Chhabra *et al.*, 2009), and the non-CAAX variant, which is not predicted to be posttranslationally modified (Figure 1). The localization pattern and cellular function of INF2–non-CAAX are not known. To understand the cellular and physiological role of INF2 in greater detail, it is important to elucidate differences in properties and roles of these two splice variants.

In this study, we show that the two splice variants of INF2 are expressed in a cell type–dependent manner. The CAAX and non-CAAX variants localize differently in cells, have different membrane association properties, and are differentially sensitive to treatments with actin- and microtubule-depolymerizing drugs. We also identify a possible role for the non-CAAX splice variant in actin-dependent maintenance of Golgi morphology.

RESULTS

INF2 displays differential localization in 3T3 and U2OS cells

We previously showed that, in Swiss 3T3 cells, INF2 localizes to the cytoplasmic face of the ER and that this ER localization depends on a C-terminal prenylation signal (CAAX box). Mutation of the cysteine in the CAAX box leads to the mislocalization of INF2 in Swiss 3T3 cells. We confirmed prenylation (farnesylation), as well as the two subsequent modifications common to prenylated proteins (peptidase removal of the C-terminal three amino acids and carboxymethylation) of INF2 immunoprecipitated from the membrane fraction of mouse brain (Figure 1B; Chhabra *et al.*, 2009).

Given these previous results, we were surprised to find that, in U2OS cells, endogenous INF2 does not localize to ER but forms a distinct, web-like pattern. Owing to its abundance, INF2 staining occasionally overlaps with ER in some places but is clearly distinct (Figure 2A). INF2 displays similar localization in HeLa cells (Supplemental Figure S1A). Suppression of INF2 expression by small interfering RNA (siRNA) in U2OS cells results in loss of the punctate staining pattern, confirming antibody specificity (Figure 8A). INF2 does localize to ER in NIH 3T3 cells (Figure 2B), similar to our previous results using Swiss 3T3 cells (Chhabra *et al.*, 2009). These differences in INF2 localization between NIH 3T3 and U2OS occur regardless of the ER marker used (Supplemental Figure S1B). Thus, INF2 displays distinct localization patterns, depending on the cell type.

Our previous studies showed that, in Swiss 3T3 cells, INF2 distribution was dramatically altered by microtubule depolymerization, collapsing around the nucleus in a similar manner to ER (Chhabra *et al.*, 2009). Because INF2 distribution differs in U2OS cells, we reasoned that the effect of microtubule depolymerization on INF2 distribution might also differ. Indeed, INF2 distribution is microtubule independent in U2OS cells, as treatment with 30 μM nocodazole for 5 or 30 min causes extensive microtubule depolymerization but does not alter INF2's web-like distribution (Supplemental Figure S2). After 1 h of nocodazole treatment, the bulk of the ER is retracted from the periphery, whereas INF2 is largely unaltered (data not shown), suggesting that the INF2 localization pattern is not dependent on weak attachment to ER.

In contrast, INF2 localization in U2OS cells is highly sensitive to drugs that cause actin depolymerization. Within 5 min of treatment

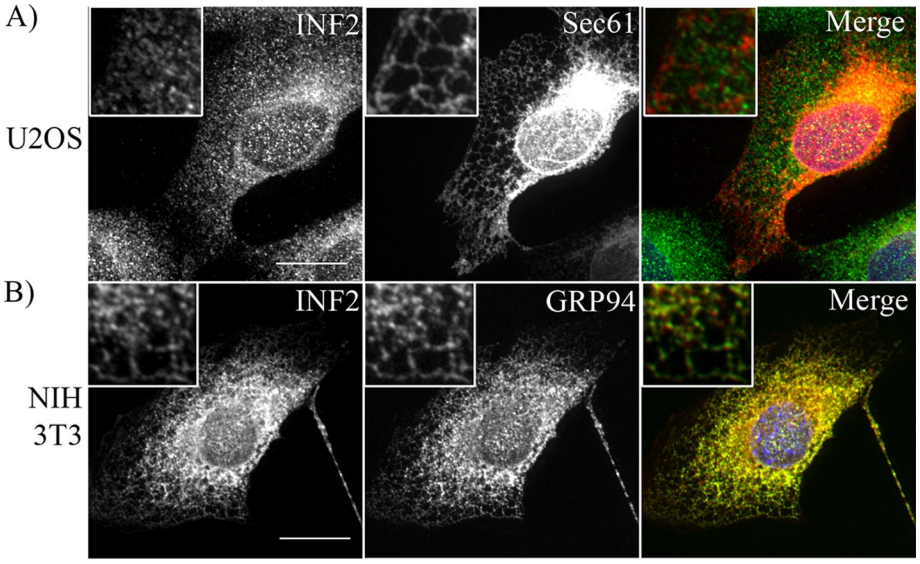

FIGURE 2: INF2 does not localize to ER in U2OS cells. (A) U2OS cells transfected with mCherry-Sec61β (an ER membrane protein; red) and stained with anti-INF2 antibody (green) and DAPI (blue). (B) NIH 3T3 cells stained with anti-INF2 (green), anti-GRP94 (an ER luminal protein; red) and DAPI (blue). See Supplemental Figure S1B for analogous INF2/ER localization using the ER marker. Scale bar, 20 μm.

with 1 μM latrunculin B (LatB), INF2 redistributes into donut-like structures in the cytoplasm (data not shown), and after 30 min INF2 has condensed further to bright cytoplasmic puncta (Figure 3A). At both time points, most INF2-enriched areas are also enriched for actin filaments, as judged by tetramethylrhodamine isothiocyanate (TRITC)–phalloidin staining. Actin stress fibers are still abundant at the 5-min time point, whereas, after 30 min of LatB treatment, cells are largely devoid of stress fibers but maintain brightly staining TRITC-phalloidin puncta of varying size. In 82% of the cases, TRITC-phalloidin puncta and INF2 puncta colocalize, with only 10% of INF2 puncta containing no TRITC-phalloidin enrichment and only 8% of TRITC-phalloidin puncta containing no INF2 enrichment (pooled data from two experiments showing similar results, 184 puncta counted). Cytochalasin D treatment has similar effects (Supplemental Figure S3). This result contrasts with our observations in Swiss 3T3 cells, in which LatB treatment does not change INF2 localization significantly (Chhabra *et al.*, 2009). Further examination of INF2 and phalloidin staining in confocal sections through the middle region of the cytoplasm suggests that the INF2 meshwork pattern overlaps with apparent actin filament staining that is distinct from the stress fiber staining that dominates the ventral regions of the cell (Figure 3B).

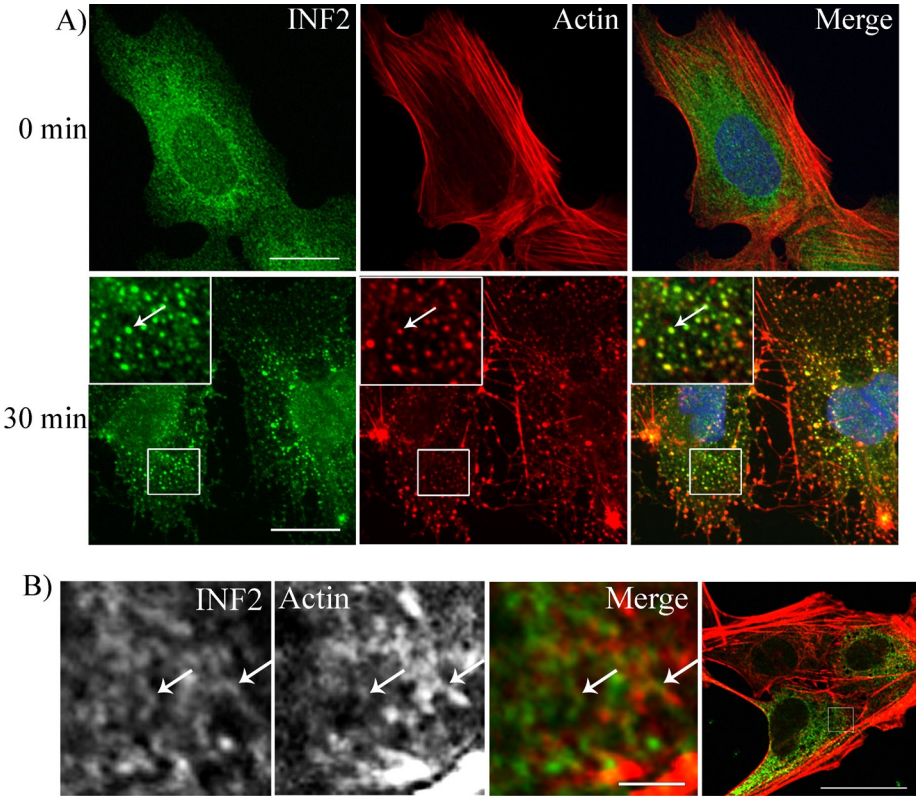

FIGURE 3: Actin depolymerization causes INF2 aggregation in U2OS cells. (A) U2OS cells were treated with 1 μM LatB for 0 and 30 min prior to fixation and staining with anti-INF2 (green), TRITC-phalloidin (red), and DAPI (blue). Arrow indicates one such actin aggregate where INF2 colocalizes. Scale bar, 20 μm. (B) Single confocal slice of U2OS cells stained with anti-INF2 (green) and rhodamine-phalloidin (red). Arrows show examples of regions where INF2 and actin filaments colocalize. Scale bars: 5 μm (leftmost three images) and 20 μm (rightmost image).

Our combined results show that INF2 distribution in U2OS cells is distinct from that in 3T3 cells, localizing in an actin-dependent, web-like pattern distinct from ER.

Cell line–specific expression patterns of INF2 splice variants

In addition to the prenylated version (INF2-CAAX), a second INF2 splice variant (INF2–non-CAAX) has been identified in cDNA libraries. INF2–non-CAAX contains an altered C-terminal region, with the 18–amino acid CAAX C-terminus being swapped for a nine–amino acid non-CAAX sequence that does not contain a prenylation sequence (Figure 1). We hypothesized that INF2's C-terminal splice variation might play a role in its cell type–specific localization. To test this hypothesis, we raised antibodies against INF2 CAAX and non-CAAX C-terminal peptides and performed Western blot analysis for these splice variants. Owing to the number of amino acid differences between the mouse and human proteins in the C-terminal region (five of 15 residues in CAAX, one of nine in non-CAAX), we produced separate antibodies to the human and mouse C-termini. Each antibody is specific for its peptide epitope, as it does not detect overexpressed green fluorescent protein fusion of the opposite isoform (Figure 4).

In NIH 3T3 cell lysates, a strong Western band for the CAAX isoform is present, whereas the non-CAAX isoform is

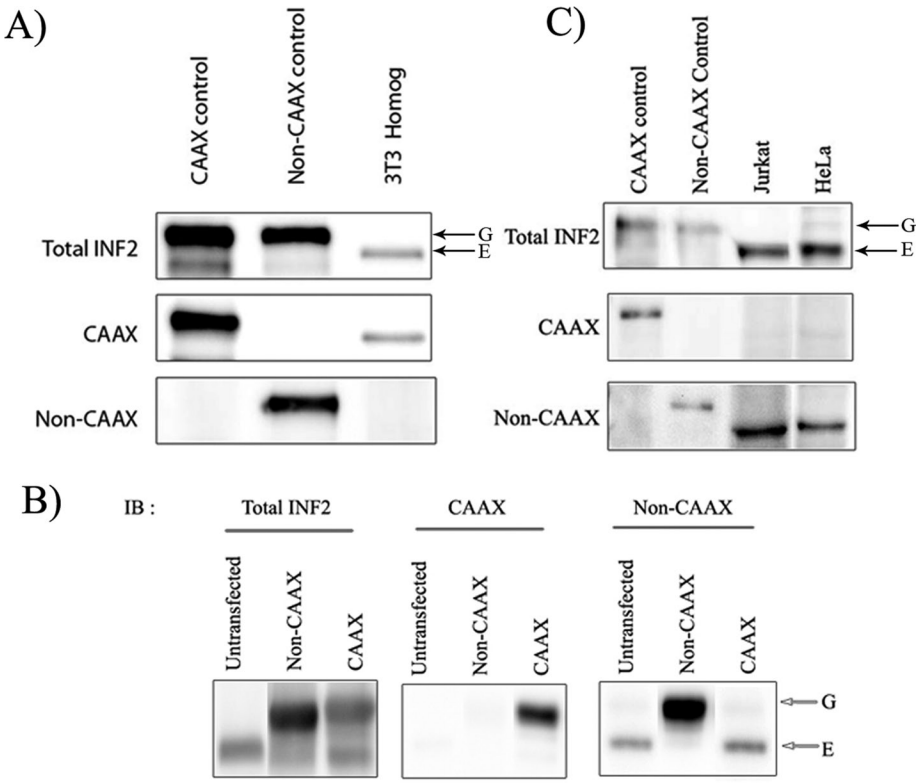

FIGURE 4: 3T3 cells express INF2-CAAX, whereas U2OS, Jurkat, and HeLa cells express INF2–non-CAAX. (A) Western blots of whole-cell homogenates from NIH 3T3 cells. CAAX and non-CAAX controls are from U2OS cells transiently transfected with GFP-tagged mouse INF2 isoforms. Western blots were probed with antibodies specific for total mouse INF2, INF2-CAAX, or INF2–non-CAAX. (B) Similar analysis as in A, using homogenates from Jurkat and HeLa cells. CAAX and non-CAAX controls are from U2OS cells transiently transfected with GFP-tagged human INF2 isoforms. (C) Western blots of immunoprecipitations of denatured lysates from U2OS cells either untransfected or stably expressing GFP-INF2-CAAX or GFP-INF2–non-CAAX. Immunoprecipitations were conducted using the total INF2 antibody. Western blots were probed with total INF2, INF2-CAAX, or INF2–non-CAAX antibodies. E, endogenous INF2; G, GFP INF2.

undetectable, suggesting that the CAAX isoform predominates in these cells (Figure 4A). We carried out similar analysis of HeLa and Jurkat lysates. In contrast to 3T3 cells, both HeLa and Jurkat lysates show clear bands for the non-CAAX isoform, with very little CAAX isoform (Figure 4B).

We conducted similar analysis on U2OS cells, with two variations: 1) as positive controls, we used U2OS cells stably transfected with GFP-INF2-CAAX or GFP-INF2–non-CAAX, and 2) we immunoprecipitated INF2 from lysates using an antibody against the FH2 domain prior to Western blotting to increase detection sensitivity. The immunoprecipitations (IPs) were conducted after rapid denaturation of total cell protein (see *Materials and Methods*) to prevent proteolysis. No detectable INF2 staining is present in the supernatants from these IPs (data not shown), suggesting that the IPs reflect the vast majority of INF2. U2OS cells show strong endogenous INF2 in the IP from untransfected U2OS cells, as well as from the stably expressing CAAX IP. These bands are also prominent when probed with the non-CAAX antibody. In contrast, there is no detectable band with the CAAX antibody (Figure 4C). This result suggests that the non-CAAX isoform predominates in these cells. Of interest, we cannot detect endogenous INF2 in the stable GFP–non-CAAX cell line, suggesting that overexpression of the non-CAAX variant causes down-regulation of endogenous INF2 protein levels.

To summarize, expression of INF2 isoforms appears to occur largely in an "either/or" manner, with 3T3 cells expressing mainly the CAAX isoform and U2OS, HeLa, and Jurkat cells expressing mainly the non-CAAX isoform. Of interest, despite undetectable expression of the INF2-CAAX protein in U2OS and Jurkat cells, RT-PCR analysis shows that both CAAX and non-CAAX messages are present (Supplemental Figure S4A).

We probed two mouse tissues with CAAX and non-CAAX antibodies: brain, since INF2 expression is high in this tissue (Chhabra *et al.*, 2009), and kidney, since INF2 mutations result in the kidney disease FSGS (Brown *et al.*, 2010). IPs of denatured whole-tissue extracts show that both CAAX and non-CAAX variants exist in mouse brain. In kidney, the CAAX variant is the predominant isoform, whereas the non-CAAX isoform is detectable but extremely weak (Supplemental Figure S4B).

The CAAX and non-CAAX isoforms differ in membrane association properties

Our immunofluorescence results show that INF2 does not localize to ER in U2OS cells but does display web-like staining, suggestive of binding to cellular structures such as membranes (Figure 2). Previously, we found that INF2 was stably associated with ER membranes in Swiss 3T3 cells, maintaining constant levels even after 120 min of digitonin permeabilization prior to fixation (Chhabra *et al.*, 2009). We conducted similar analysis on endogenous INF2 in U2OS cells, using mCherry-tagged Sec61β as an integral membrane protein control. In contrast to Swiss 3T3 cells, INF2 is depleted from digitonin-permeabilized U2OS cells almost completely within 5 min. At 30 min, there is no detectable INF2 left within cells (Figure 5). This result is similar to that obtained for GFP in these cells (data not shown). In contrast, Sec61β is retained on ER membranes throughout the experiment. Our conclusion is that, whereas the CAAX isoform is stably bound to the ER membrane, the non-CAAX isoform is loosely associated with a web-like meshwork in the cytoplasm.

To test membrane association further, we subjected cell lysates to differential centrifugation, creating low-speed pellet (LSP, 2000 × *g*), high-speed pellet (HSP, 436,000 × *g*), and high-speed supernatant (HSS) fractions. In NIH 3T3 cells, INF2 partitions primarily in the pellet fractions, distributing evenly between the LSP and the HSP, with only 3% in the HSS (Supplemental Figure S5, A and B). Probing for the CAAX isoform gives a similar distribution, whereas the non-CAAX isoform is undetectable even when the blot is overexposed and overprocessed. Calnexin, an ER transmembrane protein, also fractionates evenly between the LSP and HSP, confirming the presence of the ER in these fractions. Tubulin, however, is almost entirely in the HSS, suggesting that material in the LSP is not a result of incomplete cell lysis during homogenization. These results are similar to our previous fractionation of Swiss 3T3 cells (Chhabra *et al.*, 2009).

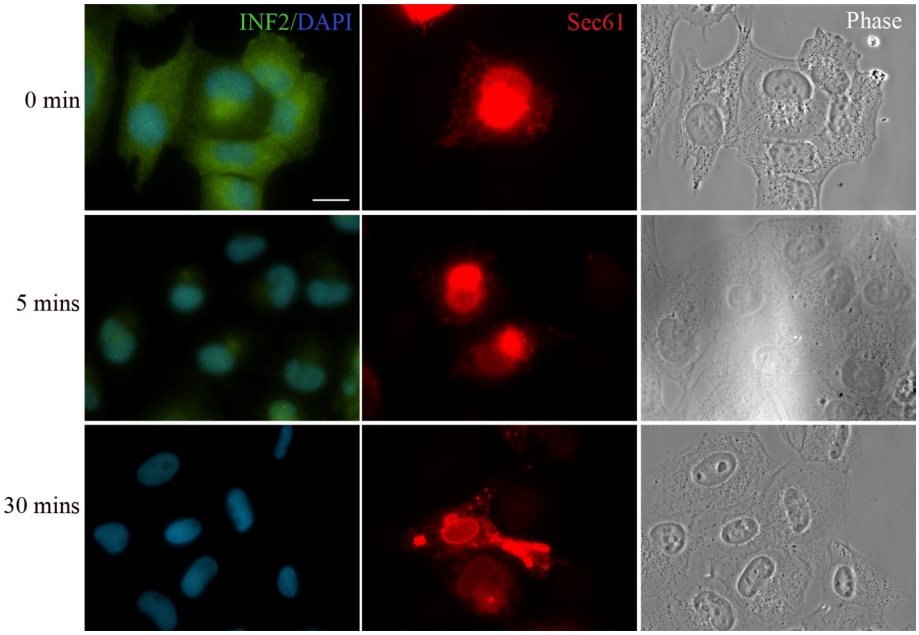

FIGURE 5: INF2 is rapidly extracted from U2OS cells. U2OS cells were permeabilized with digitonin on ice for 0, 5, and 30 min before fixation. The cells were then stained with anti-INF2 antibody (green) to detect endogenous INF2 and DAPI (blue). mCherry-Sec61β (red) was used as an ER membrane marker. Scale bar, 20 μm.

We conducted similar fractionation in HeLa and Jurkat cells, which express primarily the non-CAAX isoform (Supplemental Figure S5, C and D). In contrast to NIH 3T3 cells, 80% of INF2 is in the LSS, with only 20% in the LSP in both HeLa and Jurkat cells. Fractionation of the LSS reveals that 66.67% of the INF2 is in the HSS and 33.33% is in the HSP. Westerns for CAAX and non-CAAX isoforms suggest that the non-CAAX is overwhelmingly predominant in the HSS and HSP, with no CAAX variant detectable. The LSP fraction contains a CAAX-reactive band but no apparent non-CAAX band in both cases, suggesting that both HeLa and Jurkat cells express low levels of CAAX variant and that this variant is tightly bound to membranes. Fractionation of U2OS cells produces similar results, albeit under different extraction conditions (Supplemental Figure S5E). These findings suggest that the CAAX and the non-CAAX isoforms are fundamentally different in terms of membrane association.

We previously showed that a GFP fusion of the INF2-CAAX isoform localizes to ER in Swiss 3T3 cells. We wondered whether we would obtain similar results in U2OS cells, since these cells express very low levels of INF2-CAAX. In U2OS cells stably expressing GFP-INF2-CAAX, this isoform localizes to ER tubules, which is best appreciated in the peripheral ER (Figure 6A). In contrast, the stable GFP-INF2–non-CAAX U2OS line displays evenly distributed GFP levels throughout the cytoplasm (Figure 6A), somewhat different from the web-like appearance of endogenous INF2 (Figure 2). Neither ER nor Golgi is strongly perturbed in the GFP-INF2-CAAX or GFP-INF2–non-CAAX cell line (data not shown). Transient expression of GFP-INF2-CAAX and GFP-INF2–non-CAAX in NIH 3T3 cells provides similar results, in that the CAAX variant localizes to ER, whereas the non-CAAX variant localizes diffusely. Also similar to U2OS cells, overexpression of these proteins does not perturb ER or Golgi structure in NIH 3T3 cells (data not shown).

Using the digitonin permeabilization technique, we find that GFP-INF2-CAAX is retained on ER, whereas GFP-INF2–non-CAAX is rapidly depleted (Figure 6B). On LatB treatment, GFP-INF2–non-CAAX behaves similarly to endogenous INF2 in U2OS cells, redistributing to actin-rich puncta (Figure 6C), with 94% of INF2 puncta colocalizing with TRITC-phalloidin puncta (pooled data from two experiments showing similar results, 294 puncta counted). Overall, N-terminal GFP fusions of INF2-CAAX and INF2–non-CAAX recapitulate the properties of the endogenous proteins.

We next asked what aspect of the C-terminus dictates INF2 localization: the presence of the farnesyl modification in the CAAX variant, or specific sequence information present in the non-CAAX C-terminus. To test this distinction, we used a GFP-INF2-CAAX mutant in the prenylated C-terminal cysteine (C1246S). As found in Swiss 3T3 cells (Chhabra *et al.*, 2009), the C1246S mutant localizes diffusely in the cytoplasm. Treatment with LatB causes condensation of C1246S to actin-rich puncta in a manner indistinguishable from GFP-INF2–non-CAAX (Figure 6C). This result suggests that the crucial factor for INF2 localization is the prenyl motif, and absence of this modification causes localization similar to the non-CAAX isoform.

INF2 knockdown causes Golgi dispersal in an actin-dependent manner

INF2 interacts with MAL and MAL2, integral membrane proteins that localize to endosomal and *trans*-Golgi–derived vesicles as well as to the Golgi itself (Millan *et al.*, 1997; Puertollano and Alonso, 1999; Andres-Delgado *et al.*, 2010; Madrid *et al.*, 2010). For this reason, we examined INF2 localization in U2OS cells in more detail by acquiring confocal images of multiple z-sections. This examination shows that although INF2 staining is spread throughout the cytoplasm, it is often enriched in similar regions as the endosomal proteins Rab5a and Rab7a (Supplemental Figure S6). It is worth emphasizing that, although INF2 enrichment is in the same general area as these endosomal markers, close examination shows no clear evidence for localization to endosomal membranes.

The position of INF2 enrichment also coincides often with the position of the Golgi in U2OS cells (Figure 7). Despite this apparent enrichment around the Golgi, INF2 does not appear to be strongly associated with the Golgi, as evidenced by the following treatments. Brefeldin A or nocodazole causes dramatic Golgi dispersal but does not result in significant INF2 redistribution (Figure 7B and Supplemental Figure S6). In contrast, LatB treatment causes INF2 redistribution to actin-rich puncta that do not systematically colocalize with the Golgi (Supplemental Figure S6).

The enrichment of INF2 in the peri-Golgi region, as well as previous evidence for interactions between actin and the Golgi (Fucini *et al.*, 2000; Dubois *et al.*, 2005; Dippold *et al.*, 2009), prompted us to test the effect of INF2 knockdown on Golgi morphology. To quantify these results, we collected confocal z-stacks of the *cis*-Golgi marker GM130 and classified Golgi morphology into three categories: compact, spread, and dispersed (Figure 8C), as discussed in *Materials and Methods*. These categories are best appreciated in three-dimensional (3D) reconstructions of the z-stacks (Supplemental Movies S1–S3).

INF2 knockdown causes Golgi dispersal in U2OS cells. The majority of control U2OS cells have compact Golgi (58%), with a low

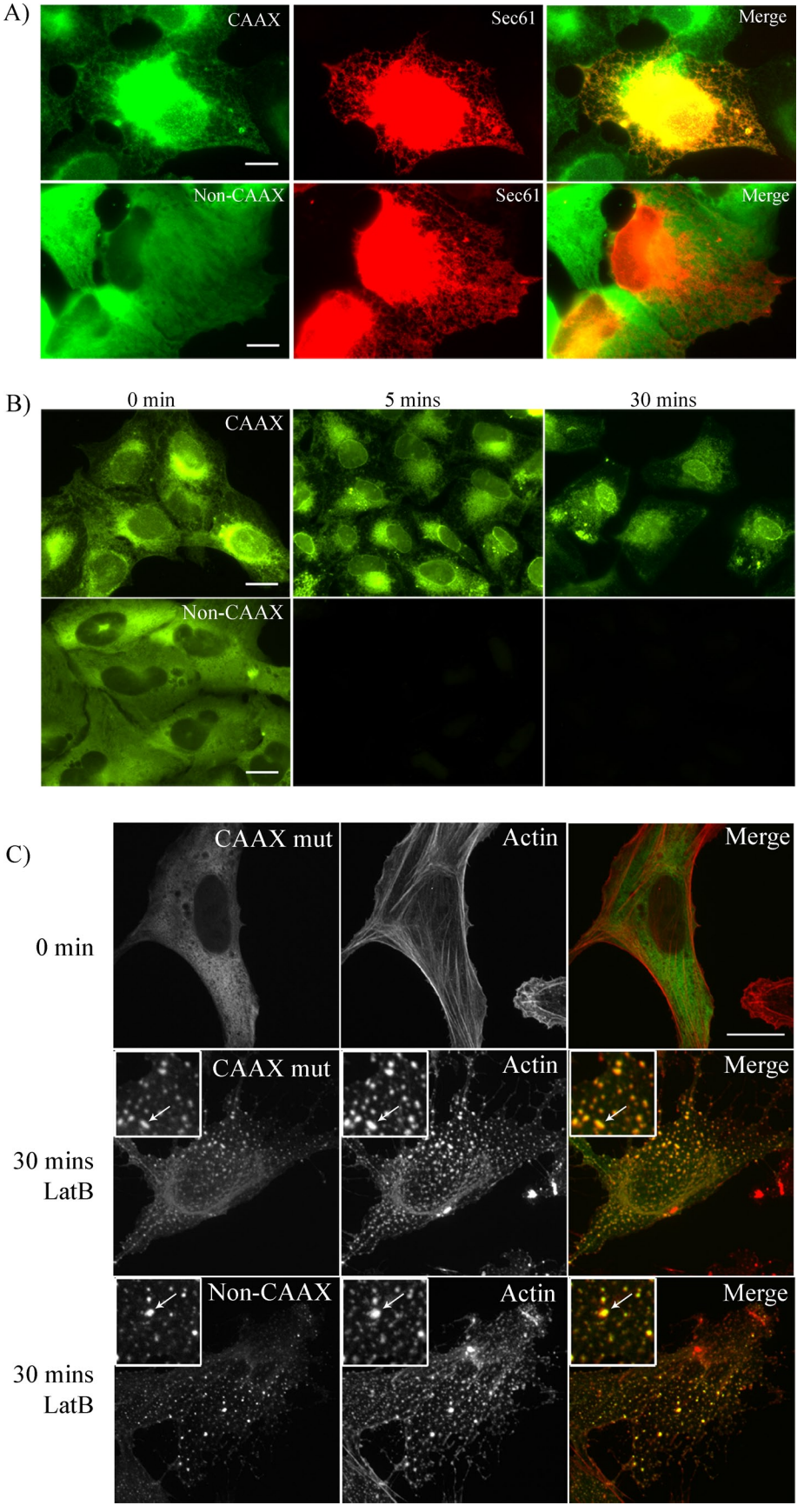

FIGURE 6: Stably transfected U2OS cells lines expressing GFP-INF2-CAAX and GFP-INF2–non-CAAX recapitulate endogenous proteins. (A) Localization of GFP-INF2-CAAX and GFP-INF2–non-CAAX in U2OS cells. mCherry-Sec61β (red) was used as an ER marker. Scale bar, 10 μm. mCherry-Sec61β was overexposed to visualize the peripheral ER. (B) Digitonin permeabilization of U2OS INF2-CAAX and non-CAAX stable cell lines. The cells were permeabilized for 0, 5, or 30 min on ice before fixation. Scale bar, 20 μm. (C) Effect of LatB on GFP-INF2-CAAX (C1246S) mutant and GFP-INF2–non-CAAX. U2OS cells were transfected with mouse GFP-INF2-CAAX mutant or GFP-INF2–non-CAAX treated with 1 μM LatB for the indicated amount of time. The cells were then fixed and stained with TRITC phalloidin. Arrow indicates one such actin aggregate where INF2 colocalizes. Scale bar, 20 μm.

percentage of dispersed Golgi (15%). Two distinct INF2 siRNAs, each inducing >80% knockdown (Figure 8B), cause a 2.5-fold drop in compact Golgi and a concomitant increase in dispersed Golgi (Figure 8D). Costaining knockdown cells with GM130 (a *cis*-Golgi protein) and golgin-97 (a *trans*-Golgi protein) reveals that the *cis*- and *trans*-Golgi remain associated in most of the dispersed Golgi fragments (Supplemental Figure 7). Similar results are obtained in HeLa cells (data not shown).

In NIH 3T3 cells, which express the CAAX isoform, the Golgi is inherently more dispersed than in U2OS cells, with 22% compact, 27% spread, and 51% dispersed in control cells. INF2 knockdown does not result in significant changes to the degree of Golgi dispersion (Supplemental Figure S8), suggesting that the CAAX isoform does not influence Golgi distribution.

We examined these effects of INF2 knockdown on the Golgi in more detail by quantifying the size of the Golgi compartment (Supplemental Figure S7B). To quantify the amount of Golgi membrane, we summed the total volume of GM130-stained structures from 3D reconstructions of z-stacks. To quantify the degree of Golgi spreading, we traced the perimeter of Golgi membranes from maximum intensity projections of z-stacks, resulting in an area including Golgi membranes and interspersed cytosol. We conducted similar measurements on nuclear volume and area from 4′,6-diamidino-2-phenylindole (DAPI) stain. These measurements show that INF2 knockdown in U2OS cells causes a slight decrease in Golgi membrane volume (63.1 ± 8.7 μm^3 for control vs. 52.7 ± 4.9 and 55.4 ± 3.3 μm^3 for INF2 knockdown) but an expansion of the Golgi spread area (87.5 ± 23.2 μm^2 for control vs. 126.9 ± 19.4 and 144.5 ±13.2 μm^2 for INF2 knockdown). In NIH 3T3 cells, the Golgi occupies a significantly greater area (164.86 ± 19.5 μm^2, 1.88-fold increase)

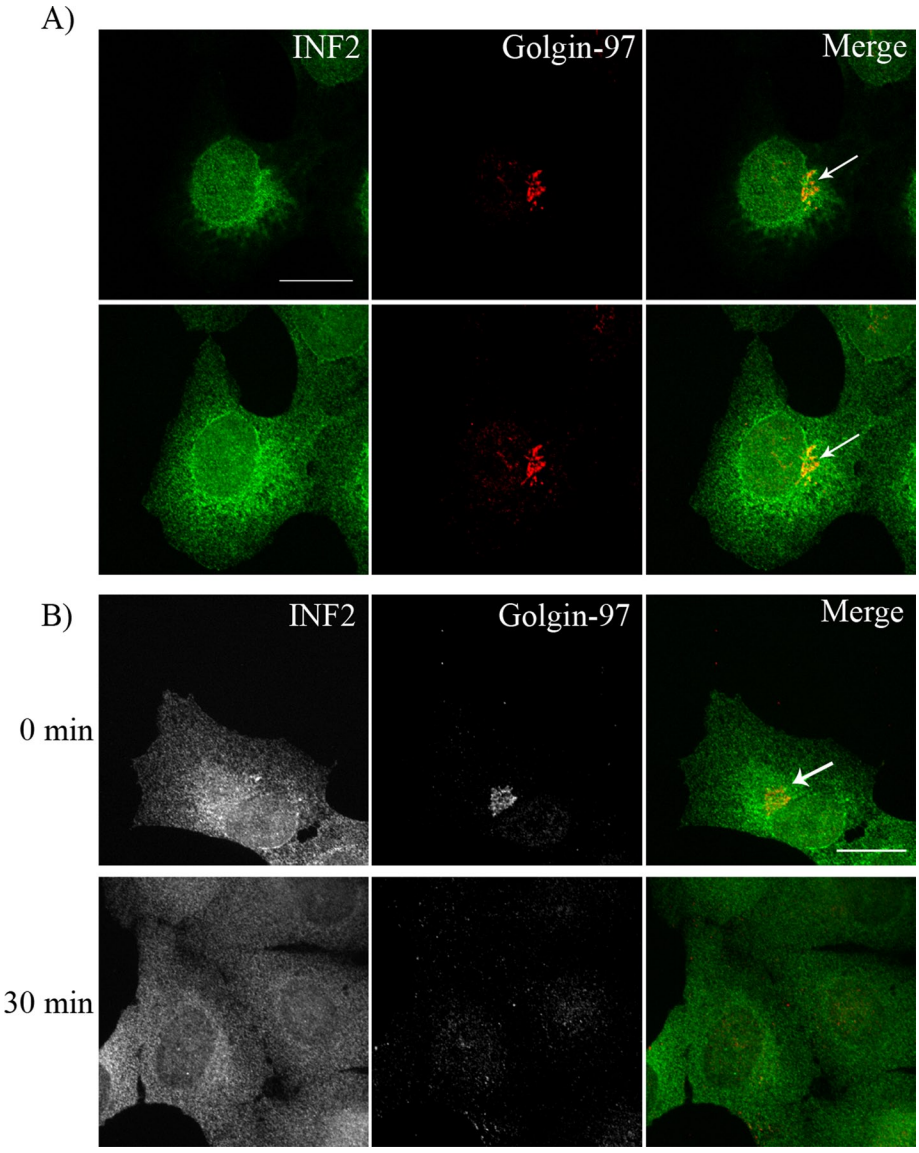

FIGURE 7: INF2 enriches around the Golgi apparatus. (A) U2OS cells were stained with anti-INF2 (green) and golgin-97 (a marker for the *trans*-Golgi network; red). Top, one confocal z-section. Bottom, the maximum-intensity projection of multiple confocal z-sections. Arrow represents INF2 enrichment around the Golgi. Scale bar, 20 μm. (B) U2OS cells treated for 0 or 30 min with 2.5 μg/ml brefeldin A. Arrow represents INF2 enrichment around the Golgi The cells were then fixed and stained with anti-INF2 (green) and anti–golgin-97 (red) antibodies. Scale bar, 20 μm.

and membrane volume (96.8 ± 13.7 μm^3, 1.53-fold increase) than in U2OS cells, but both values decrease slightly upon INF2 knockdown. Exogenous expression of an siRNA-resistant INF2–non-CAAX construct causes partial rescue of the siRNA-induced Golgi expansion phenotype (Golgi area, 45 ± 5 μm^2 for control,154 ± 23 μm^2 for INF2 knockdown, and 84 ±12 μm^2 for INF2 knockdown/reexpression).

To examine whether the Golgi dispersion observed upon INF2 knockdown depends on the actin cytoskeleton, we treated control and INF2-depleted U2OS cells with LatB prior to examination of Golgi morphology. In control cells, LatB treatment results in elimination of dispersed Golgi and a large reduction in spread Golgi (Figure 8E) while having no apparent effect on ER morphology (data not shown). Golgi compaction upon LatB treatment is rapid, with noticeable compaction at 10 min and full compaction occurring by 30 min (Supplemental Figure S7B). Even though total cell area also shrinks during this time course (Supplemental Figure S7), the effects on Golgi do not appear to be due to overall shrinking of cellular area, since Golgi compaction occurs in cells that are still well spread (Supplemental Figure S7C). This effect on Golgi occurs also in INF2-depleted cells, which have greatly increased spread Golgi in the absence of LatB (Figure 8E and Supplemental Figure S7B). These results suggest that Golgi dispersion in U2OS cells is actin dependent and that INF2's role is to counteract this actin-dependent dispersion.

One question from these results concerns whether INF2 knockdown produces any observable effect on actin in the vicinity of the Golgi. To address this question, we costained U2OS cells with GM130 and TRITC-phalloidin after transfection with control siRNA or INF2 siRNA. Careful examination reveals the presence of TRITC-phalloidin patches apparently intermingled with Golgi (Figure 9A; also see Supplemental Movies S4 and S5 for examination of z-stacks). These patches are largely obscured by ventral stress fibers in wide-field fluorescence images, and z-sectioning is necessary to view them clearly. The patches vary in size and intensity but are generally <1 μm in diameter. On INF2 knockdown, the patches disperse along with Golgi, and the number of patches is reduced by ~30%. Control cells contain 12.7 patches/Golgi (217 patches from 17 cells), whereas INF2 siRNA cells contain 9.0 patches/Golgi (190 patches from 21 cells; two experiments conducted, both giving a similar 30% decrease). Costaining for INF2, actin filaments, and Golgi reveals that 72% of the patches have visible INF2 staining (Figure 9B).

One possibility is that INF2 knockdown alters Golgi morphology indirectly by altering the cell cycle, since Golgi morphology changes during the cell cycle (Lippincott-Schwartz and Zaal, 2000). Experiments using flow cytometric measurement of DNA content show no clear change in cell cycle upon INF2 knockdown (data not shown). To test the effects of INF2 knockdown on Golgi at a particular cell cycle stage, we synchronized U2OS cells by low-dose nocodazole treatment followed by mitotic shake-off and 6 h of recovery, resulting in a G1-synchronized population. In these synchronized cells, INF2 knockdown results in a similar increase in spread and dispersed cells as observed in nonsynchronized cells (83% compact vs. 17% spread vs. 0% dispersed cells in control [48 cells counted] compared to 39 vs. 49 vs. 12% in INF2 siRNA1 cells [49 cells counted]).

DISCUSSION

In this study, we find significant differences in cellular localization, expression patterns, and cellular function between two splice variants of the formin INF2. The CAAX variant, which is farnesylated at

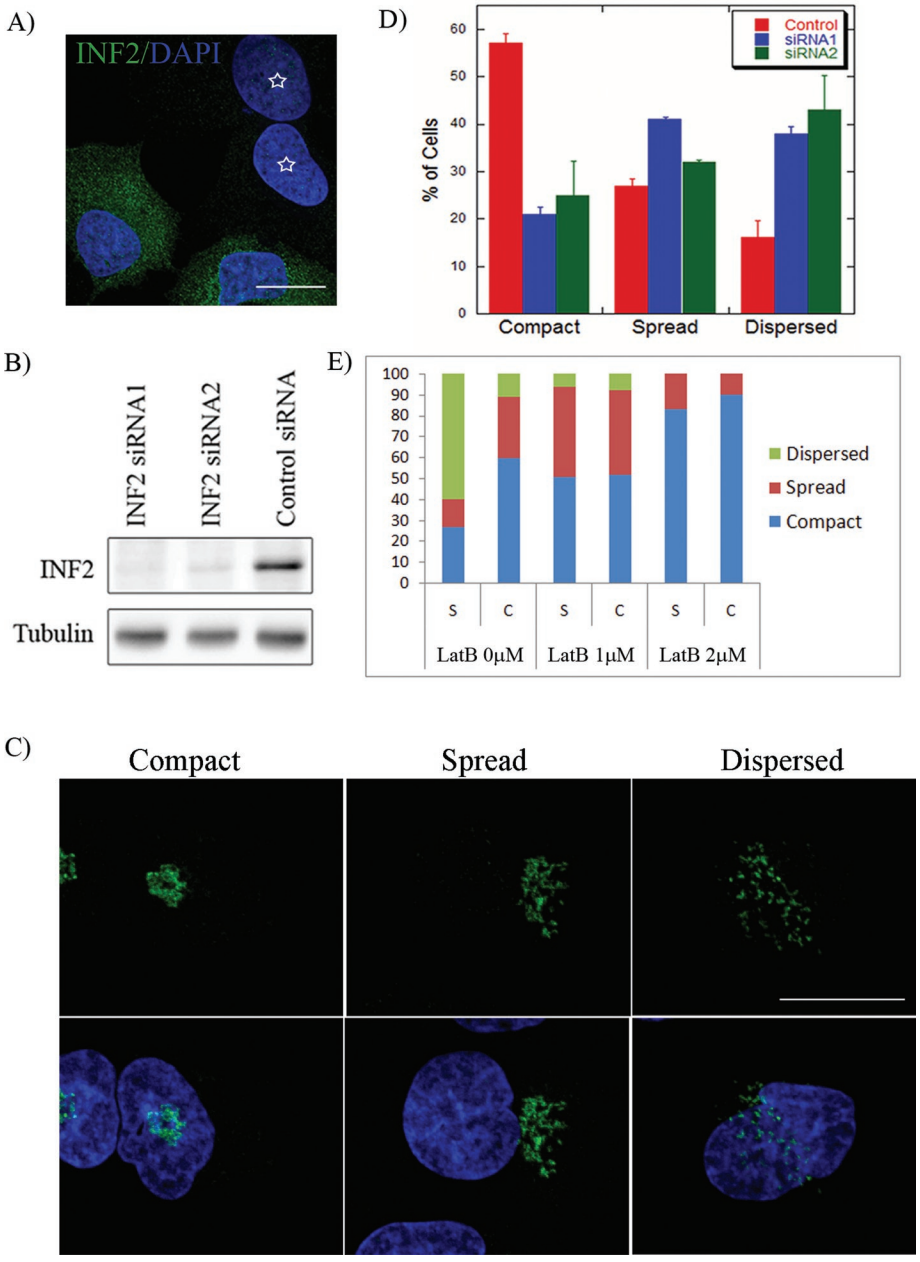

FIGURE 8: INF2 depletion causes dispersal of the Golgi apparatus in U2OS cells. (A) INF2-depleted U2OS cells stained with anti-INF2 (green) and DAPI (blue). The stars indicate cells that have been knocked down. Scale bar, 20 μm. (B) Western blot showing INF2 depletion using two different siRNAs. Tubulin was used as a loading control. (C) Representative images of compact, spread, and dispersed Golgi. GM130 (green) was used as the Golgi marker. DAPI is in blue. Scale bar, 20 μm. (D) Quantification of Golgi dispersion. The data represent the average of three independent experiments (n > 200 cells). Error bars, SE. (E) Quantification of Golgi morphology upon INF2 depletion and LatB treatment. C, control siRNA; S, INF2 siRNA. Cells were treated with 0, 1, or 2 μM LatB for 1 h prior to fixation.

its C-terminus, is stably bound to ER membranes (Chhabra *et al.*, 2009; the present study). Although microtubule depolymerization disrupts INF2-CAAX distribution (along with ER), actin depolymerization has no apparent effect. In contrast, the non-CAAX variant displays a web-like cytoplasmic appearance that is distinct from ER. Although INF2-non-CAAX localization is unaffected by microtubule depolymerization, actin depolymerization causes collapse of INF2 into discrete puncta that generally enrich with residual actin filaments. The fact that a fraction of INF2–non-CAAX partitions to the pellet fraction upon differential centrifugation of cell lysates suggests that INF2–non-CAAX is at least weakly associated with membranes or other pelletable cellular structures.

INF2 splice variants are differentially expressed in cell lines. Whereas the CAAX variant predominates in NIH 3T3 cells, non-CAAX is the major variant in U2OS, HeLa, and Jurkat cells. Tissues such as brain and kidney express both variants to various degrees. Future experiments will determine whether specific cell types in these tissues (neurons, astrocytes, podocytes) express only one splice variant.

An interesting feature of INF2 expression is that, although U2OS cells do not express detectable INF2-CAAX protein, they do express both CAAX and non-CAAX mRNA. This finding suggests that splice variant regulation may take place at a translational level. Also intriguing in this regard is that our stably transfected GFP-INF2–non-CAAX U2OS cell line appears to suppress the production of endogenous INF2–non-CAAX protein, whereas our stable GFP-INF2-CAAX U2OS line does not. These findings suggest possible mechanisms controlling INF2 splice variant expression. In this respect, it might be noteworthy that the mRNA for another formin, mDia1, is localized to the ER in a translation-dependent manner (Liao *et al.*, 2011).

The localization of INF2–non-CAAX in a web-like network, distinct from ER, is intriguing. INF2 is rapidly extracted from this network, suggesting that it is loosely attached or that the network is labile. INF2 organization in this web-like pattern is actin dependent, since LatB treatment dramatically alters INF2 distribution. We wonder whether this finding suggests an actin network in interphase cells, similar to those identified in meiotic oocytes (Lenart *et al.*, 2005; Li *et al.*, 2008; Schuh and Ellenberg, 2008). We have been unable to identify actin filaments adopting this web-like structure using fluorescent phalloidin staining, but the presence of abundant stress fibers complicates visualization of less abundant structures. We point out that it is not clear at this point that the web-like, INF2-containing structure contains a membrane component.

The CAAX and non-CAAX variants also have functional differences. Knockdown of INF2 in U2OS cells, which express primarily the non-CAAX variant, has a dramatic effect on Golgi structure, causing transition from its normally compact structure to dispersed Golgi fragments. Of interest, these fragments appear to maintain association of *cis* and *trans* membranes despite their dispersal. In addition, the dispersed Golgi remains largely perinuclear and does not spread to more peripheral regions. However, we do not observe a change in Golgi morphology upon INF2 depletion in NIH 3T3

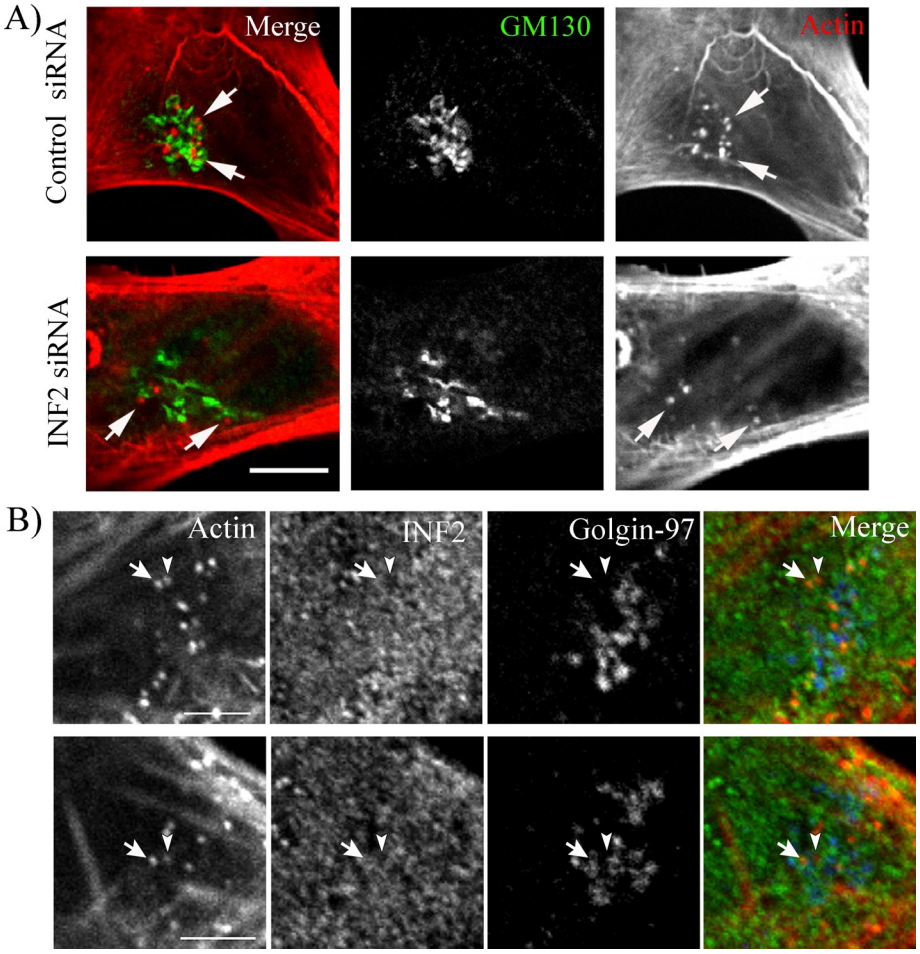

FIGURE 9: Peri-Golgi actin patches are reduced and dispersed in INF2 knockdown. (A) Cells transfected with control (top) or INF2 (bottom) siRNAs were fixed and stained with anti-GM130 (green) and TRITC-phalloidin (red). Maximum-intensity projections of three consecutive 0.2-μm sections taken through the middle of Golgi region are shown. Arrows indicate actin patches found in close proximity to Golgi stacks. Scale bar, 10 μm. Quantification of peri-Golgi actin patches reveals an approximate 30% decrease in patch number upon INF2 knockdown (12.7 patches/Golgi in control siRNA [217 patches in 17 cells] vs. 9.0 in INF2 siRNA [190 patches in 21 cells]). Quantification is the result of two separate experiments that showed similar 30% decrease for INF2 siRNA. (B) Colocalization of INF2 with actin patches. Single confocal slice of U2OS stained with anti-INF2 (green), TRITC-phalloidin (red), and anti–golgin-97 (blue). Arrow indicates a patch that colocalizes with INF2, and arrowhead indicates a patch that does not colocalize with INF2. Scale bar, 5 μm.

cells, which expresses the CAAX variant predominately. The fact that INF2-CAAX localizes to ER and that overexpression of a mutant INF2-CAAX construct incapable of DID/DAD interaction or effective depolymerization causes ER collapse (Chhabra *et al.*, 2009) also suggests a fundamentally distinct cellular function.

A growing number of studies point strongly to an association between actin and Golgi. There is evidence for an actin network surrounding portions of the Golgi (Beck and Nelson, 1998; Holleran and Holzbaur, 1998), and both spectrin/actin and Arp2/3 complex–mediated actin have been identified on Golgi (Devarajan *et al.*, 1996; Beck *et al.*, 1997; Chen *et al.*, 2004). Two Arp2/3 complex activators, WHAMM and WAVE complex (Kondylis *et al.*, 2007; Campellone *et al.*, 2008), associate with Golgi. Colfilin also associates with the Golgi and plays a role in cargo sorting (von Blume *et al.*, 2009, 2011). Finally, a number of myosins localize to Golgi (Allan *et al.*, 2002), and suppression of myosin 18A causes Golgi compaction (Dippold *et al.*, 2009), suggesting that this myosin might mediate a dispersive force for Golgi, although recent work suggests that *Drosophila* myosin 18A does not act as an actin-based motor in vitro (Guzik-Lendrum *et al.*, 2011).

How do actin filaments influence Golgi structure, and what role does INF2 play in this process? We can envision several possible roles for INF2 in this respect, including the following: 1) INF2 acts to polymerize cytoplasmic actin, and these filaments serve to confine Golgi; 2) INF2 acts to depolymerize actin filaments that serve as tracks for myosin-mediated Golgi dispersion (Dippold *et al.*, 2009); or 3) a low percentage of INF2 molecules acts directly on the Golgi to polymerize or depolymerize Golgi-associated actin filaments. Our data provide suggestions but do not distinguish clearly among these possibilities. First, INF2–non-CAAX does not noticeably associate with Golgi but does so in a more general meshwork pattern that enriches somewhat near Golgi. Second, the effect of INF2 knockdown on Golgi dispersal is counteracted by LatB treatment, possibly suggesting that INF2's role involves actin depolymerization. Transient actin networks exist in oocytes to move meiotic chromosomes (Lenart *et al.*, 2005; Li *et al.*, 2008; Schuh and Ellenberg, 2008), and we raise the possibility that a similar network might exist in interphase cells. However, we also identify actin filament patches in the vicinity of the Golgi and show that INF2 knockdown causes dispersion and decrease in these patches. The question of how these patches might relate to Golgi morphology is unclear, although similar patches have been identified using live-cell microscopy and actin filament–binding probes (Miserey-Lenkei *et al.*, 2010; Almeida *et al.*, 2011). The relationship of these patches with INF2, which localizes in more of a meshwork pattern but does enrich on the majority of these patches, also remains to be elucidated.

Recent publications have shown that two other formins, FMNL1 (Colon-Franco *et al.*, 2011) and mDia1 (Zilberman *et al.*, 2011), have effects on Golgi structure. The gamma splice variant of FMNL1 enriches strongly at Golgi, and FMNL1 suppression results in Golgi dispersion. In contrast, mDia1 suppression results in Golgi compaction, although, like INF2, mDia1 is not enriched on Golgi membranes. Of interest, mDia1 appears to have effects on Golgi fusion, with overexpression of mDia1-suppressing fusion. There may be a direct relationship between INF2 and mDia1, since the two proteins interact and since INF2 can inhibit actin polymerization by mDia1 (Sun *et al.*, 2011). This relationship may result in an intricate control of cytoplasmic actin polymerization, with one consequence being control of Golgi structure. Overall, the contributions of multiple formin proteins in controlling Golgi structure is an intriguing subject for future research and might suggest that multiple actin-based processes are involved.

It is also possible that INF2's effects on the Golgi involve microtubules, which are necessary for Golgi compaction (Cole *et al.*, 1996). Other formins have been shown to interact with microtubules (Bartolini *et al.*, 2008; Bartolini and Gundersen, 2010), and we found that INF2 can both bind and bundle microtubules in vitro (Gaillard *et al.*, 2011).

Our findings add information to recently published work on INF2 function in the secretory pathway. In polarized cell lines such as HepG2 and MDCK cells, INF2 plays a role in basolateral-to-apical transcytosis (Madrid *et al.*, 2010). In Jurkat T cells, INF2 plays a role in the transport of LCK kinase to the plasma membrane (Andres-Delgado *et al.*, 2010). In both cases, INF2's function depends on interaction with a member of the MAL family of proteins—integral membrane proteins that localize to the *trans*-Golgi and endosomal pathway and have been previously shown to be important in Golgi-to-apical transport in epithelial cells (Millan *et al.*, 1997; Puertollano and Alonso, 1999).

To interpret mechanistic roles for INF2 in these processes, an understanding of the splice variants present in the particular cells in question is crucial. The INF2/MAL interaction requires INF2 sequence C-terminal to the DAD (Andres-Delgado *et al.*, 2010; Madrid *et al.*, 2010), but both CAAX and non-CAAX variants can interact by two-hybrid assay, so in principle either splice variant could act in the MAL pathway. Our study reveals that the non-CAAX variant predominates in Jurkat cells. Live-cell microscopy of MAL and Lck dynamics in Jurkat cells shows vesicles emanating from intense pericentriolar staining and moving to the periphery (Andres-Delgado *et al.*, 2010). In the INF2 knockdown cells, the pericentriolar staining persists, but vesicles containing MAL and Lck no longer move to the periphery. We wonder whether the transport defect is due in part to a Golgi defect, in addition to roles on endosomes in these cells.

MATERIALS AND METHODS

DNA constructs

Human INF2 ORF clone (SC313010) was obtained from OriGene (Rockville, MD). The gene was amplified using a GC-RICH PCR system (Roche, Indianapolis, IN) and subcloned into eGFP-C1 vector (Clontech, Mountain View, CA) between *Xho*I and *Eco*RI sites. Similarly, INF2–full-CAAX (amino acids 1–1249) and INF2–full-non-CAAX (amino acids 1–1240) were generated by PCR and cloned into eGFP-C1 between *Xho*I and *Eco*RI sites. The C1246S mutation was made in the INF2–full-CAAX construct using QuikChange mutagenesis (Stratagene, Santa Clara, CA). The mCherry-Sec61β was a kind gift from Jennifer Lippincott-Schwartz (National Institute of General Medical Sciences, Bethesda, MD). The GFP-ER construct, containing the ER-targeting sequence (amino acids 233–250) of budding yeast UBC6 (Wozniak *et al.*, 2009), was a kind gift from Victoria Allan (University of Manchester, Manchester, United Kingdom).

RT-PCR

mRNA was isolated from cells using TRIzol reagent and cDNA synthesized using SuperScript III as per the manufacturer's protocol (Invitrogen, Carlsbad, CA). Because the CAAX exon is 5′ to the non-CAAX exon and the non-CAAX exon is retained in the CAAX mRNA, we designed primers to detect both CAAX and non-CAAX isoforms by synthesizing a sense oligo in the exon preceding the CAAX exon and an antisense primer in the non-CAAX exon. The primers used for human INF2 were as follows: forward, 5′CGGTGACTCTGGGAGATGCTCAG3′; reverse, 5′TCACTTGGCCTTGGGCCTGGGCC3′; they gave fragments of 477 bases for CAAX and 420 bases for non-CAAX. PCR reactions were conducted using Taq (Invitrogen).

Cell culture and plasmid transfections

NIH 3T3, HeLa, and U2OS cells were maintained in DMEM with 4.5 g/l glucose, 584.0 mg/l L-glutamine, 110.0 mg/l sodium pyruvate, and 10% calf serum (Atlanta Biologicals, Lawrenceville, GA). NIH 3T3 cells were a kind gift from Gregg Gundersen (Columbia University, New York, NY). HeLa cells were obtained from the American Type Culture Collection (ATTC, Manassas, VA), and U2OS cells were a kind gift from Duane Compton (Dartmouth Medical School). Jurkat T leukemic cells were obtained from ATCC and cultured in RPMI 1640 with L-glutamine, 5% fetal bovine serum (Atlanta Biologicals), 1 mM sodium pyruvate, 2.5 mg/ml glucose, and 0.05 mM 2-mercaptoethanol. All cells were maintained at 37°C and 5% CO_2. Lipofectamine 2000 (Invitrogen) was used for all plasmid transfections as per the manufacturer's protocol. A total of 100 ng of each plasmid DNA was used for all transfections, and the cells were analyzed 24 h posttransfection.

Antibodies

Polyclonal antibodies against INF2-FH1-FH2-C (amino acids 469–1249) were raised in rabbits by Covance (Denver, PA) and affinity purified by using INF2-(C) (amino acids 941–1249) or INF2-(FH1-FH2) (amino acids 469–940) coupled to Sulfolink (Pierce, Thermo Fisher Scientific, Rockford, IL). To generate splice variant–specific antibodies, human INF2 CAAX (acetyl-EEVPPDSDDNKTKKLC-amide) or non-CAAX (acetyl-CQEGLRPRPKAK) peptides (Figure 2) coupled to KLH were injected into rabbits by Covance. The serum was purified using Sulfolink beads coupled to the CAAX or non-CAAX peptides. A similar procedure was used for mouse splice variants, using acetyl-QEEFVPDSDDIKAKRLC-amide (CAAX) or acetyl-CEGLRSRPKAK (non-CAAX).

Anti-tubulin (DM1-α; Sigma-Aldrich, St. Louis, MO) was used at 1:10,000 dilution. GRP94 was detected using a rabbit polyclonal antibody (SPA-851; Stressgen, San Diego, CA) at 1:500 dilution. GM130 (ab52649; Abcam, Cambridge, MA) was stained using a polyclonal antibody at 1:300 dilution. Golgin-97 was detected using a monoclonal antibody (A21270; Invitrogen) at 1:300 dilution.

Secondary antibodies used were fluorescein and Texas red–conjugated anti–rabbit immunoglobulin G (IgG; Vector Laboratories, Burlingame, CA), Texas red (Vector Laboratories), and Alexa Fluor 405–conjugated anti–mouse IgG (Invitrogen).

Fluorescence microscopy

Cells were fixed with 4% formaldehyde in phosphate-buffered saline (PBS) for 1 h at room temperature. After washing with PBS, the cells were permeabilized on ice with 0.25% Triton X-100 in PBS for 15 min. Cells were then washed with PBS prior to blocking with 2.5% calf serum in PBS for 1 h at room temperature. For INF2 staining, either unlabeled rabbit anti-INF2 at 5 µg/ml or Cy3-labeled rabbit anti-INF2 at 5 µg/ml was used. All primary staining was conducted for 1 h at room temperature. Following another wash with PBS, the secondary antibodies were added for 1 h at room temperature. For nuclear staining, DAPI was used for 10 min at 1:250,000 dilution. Actin was stained using 100 nM TRITC-phalloidin (Sigma-Aldrich). In cases in which Cy3-labeled anti-INF2 was used, cells were treated with the Cy3-labeled antibody subsequent to the secondary antibody incubation for 1 h. We found that the anti-INF2 antibody did not stain cells well after fixation in glutaraldehyde or methanol.

Images were captured using a Wave FX spinning disk confocal system (Quorum Technologies, Guelph, Canada; on a Nikon [Melville, NY] Eclipse microscope), using a 491-nm laser and 525/20 filter for GFP, a 403-nm laser and 460/20 filter for DAPI, and a 561-nm laser and 593/40 filter for Texas red. Images were acquired using

MetaMorph and were processed using Nikon Elements and Photoshop CS (Adobe, San Jose, CA).

Digitonin permeabilization

U2OS cells were plated overnight onto 18-mm glass coverslips. Coverslips were washed several times in ice-cold PBS and then extracted with EB (50 mM 4-(2-hydroxyethyl)-1-piperazineethanesulfonic acid [HEPES], pH 7.5, 5 mM ethylene glycol tetraacetic acid, 1 mM $MgCl_2$, 1 mM dithiothreitol [DTT], 1 pill/50 ml Roche Complete Protease Inhibitor without EDTA) with 0.15 mM digitonin (300410; Calbiochem, La Jolla, CA) on ice for the indicated time. Cells were then fixed and processed for fluorescence microscopy as described earlier.

Subcellular fractionation and Western blotting

The entire procedure was conducted on ice or at 4°C. Cells at ~80% confluence were washed several times in iced PBS and once with EB and then were scraped in 1 ml of EB per 100-mm plate. Cells were homogenized 30 times in a stainless steel Dura-Grind (Wheaton Instruments, Millville, NJ). KCl was added to 50 mM after homogenization. The homogenate was centrifuged 10 min at 2000 × *g* in a swinging bucket rotor. The supernatant (LSS) was centrifuged for 20 min at 100,000 rpm (436,000 × *g* max) in a TLA120.2 centrifuge (Beckman Coulter, Brea, CA). Both pellets from the 2000 × *g* spin (LSP) and the 436,000 × *g* spin (HSP) were washed once in EB with 50 mM KCl and then resuspended in EB plus 50 mM KCl. To prepare samples for SDS–PAGE, 50 µl was mixed with 34 µl of 10% SDS and 1 µl of 1 M DTT, boiled 5 min, and cooled to 23°C; then 17 µl of 300 mM of freshly made *N*-ethylmaleimide (NEM; Pierce) in water was added. Just before SDS–PAGE, the protein sample was mixed 1:1 with 2× DB (250 mM Tris-HCl, pH 6.8, 2 mM EDTA, 20% glycerol, 0.8% SDS, 0.02% bromophenol blue, 1000 mM NaCl, 4 M urea). We found that these sample preparation conditions were essential in obtaining a single protein band by Western blotting. If extraction was in normal SDS–PAGE buffer (containing 0.4% SDS, with no cysteine alkylation), we obtained multiple bands of apparent lower mass, as well as significant staining at very high apparent mass.

For IPs, U2OS cells (100-mm plate at 80% confluence) were lysed at room temperature in 1 ml of an IP buffer containing 100 mM HEPES (pH 7.4), 200 nM NaCl, 1 mM $MgCl_2$, 4 mM EDTA, 2.5% SDS, Complete Protease Inhibitor, and 10 mM DTT. Lysates were immediately boiled for 5 min and cooled for 1 min in 23°C water; then 100 µl of 300 mM NEM (freshly made) was added. Thesit (P-9641; Sigma-Aldrich) was added to 8% and then the sample was centrifuged at 100,000 rpm for 20 min in a TLA120 rotor. The resulting homogenates were precleared using protein A–Sepharose beads (GE Biosciences, Piscataway, NJ) for 2 h at 4°C. The IPs were carried out overnight at 4°C using 2 µg of the appropriate antibody and 10 µl of protein A–Sepharose beads milliliter of homogenate. The beads were washed multiple times with IP buffer (lacking the SDS and DTT but containing 1% thesit) before being processed for SDS–PAGE and Western blotting as described.

Proteins were separated by 7.5% SDS–PAGE and transferred to a polyvinylidene fluoride membrane (Millipore, Billerica, MA). The membrane was blocked with TBS-T (20 mM Tris-HCl, pH 7.6, 136 mM NaCl, and 0.1% Tween-20) containing 3% bovine serum albumin (Research Organics) for 1 h and then incubated with the primary antibody solution at 4°C overnight. After washing with TBS-T, the membrane was incubated with horseradish peroxidase (HRP)-conjugated secondary antibody (Bio-Rad, Hercules, CA) for 1 h at room temperature. Signals were detected by chemiluminescence (Pierce).

INF2 knockdown

All siRNAs were ordered from Applied Biosystems/Ambion (Austin, TX). The sequences were as follows: INF2 siRNA1, 5′CCAUGAAGGCUUUCCGGGA3′; siRNA2; 5′CUUGGCAUCACAUCAACA3′. Ambion negative control 1 (AM4635) was used as the control siRNA. U2OS cells were transfected using Lipofectamine RNAimax (Invitrogen) with 50 nM of the siRNA as per the manufacturer's protocol. At 96 h posttransfection, the cells were used for analysis. NIH 3T3 cells were transfected using Lipofectamine 2000 and PLUS Reagent (Invitrogen) with 200 nM siRNA.

Golgi dispersal analysis

Cells were fixed and stained for GM130 as described. Maximum intensity projections and 3D reconstructions of confocal z-stacks were used (0.2-µm slices, 20–30 z-slices, depending on cell height). Golgi structure was classified into three categories: compact (covering less than one-fourth of the nuclear perimeter), spread (between one-fourth and one-half of the nuclear perimeter), and dispersed greater than one-half of nuclear perimeter). Images were analyzed by two or three blinded observers, and the results are from three independent experiments.

U2OS synchronization and DNA content analysis

U2OS cells were plated in six-well plates and transfected with control siRNA or INF2 siRNA. Three days posttransfection, when the cells were ~80% confluent, the medium was replaced with DMEM with 50 ng/ml nocodazole for 13–16 h. Mitotic cells were then isolated by mitotic shake-off (gentle shake and tapping the plate). Mitotic cells were concentrated by centrifuging at 300 × *g* for 10 min, washing with fresh medium, and plating on poly-L-lysine–coated coverslips. After 6 h of culturing, all cells had entered G1 phase, as judged by DNA content analysis.

For DNA content analysis, cells were trypsinized and centrifuged 5 min at 300 × *g*. The pellet was resuspended in cold PBS and centrifuged again. Supernatant was removed, and the cell pellet was resuspended in 0.5 ml of cold PBS. For fixation, 4.5 ml of 70% ice-cold ethanol was added dropwise to the cell suspension while vortexing at high speed. For staining, cells were washed twice with PBS and resuspended in 1 ml of propidium iodide/RNase staining solution containing 20 µg/ml propidium iodide, 0.1% Triton X-100, and 0.2 mg/ml RNaseA (RNase A from Calbiochem) for 30 min at 23°C. The cells were analyzed by fluorescence-activated cell sorting using a FACSCalibur flow cytometer and Cell Quest software (BD Biosciences, Rockville, MD). Populations of cells were gated according to the fluorescence intensity of PI staining.

ACKNOWLEDGMENTS

We thank Gregg Gundersen (Columbia University), Duane Compton (Dartmouth Medical School), Victoria Allan (University of Manchester), and Jennifer Lippincott-Schwartz (National Institute of General Medical Sciences) for cell lines and plasmids. We thank Li Gog for directing traffic. This work was supported by National Institutes of Health Grants R01 GM069818R01 DK088826 and the Hitchcock Foundation.

REFERENCES

Allan VJ, Thompson HM, McNiven MA (2002). Motoring around the Golgi. Nat Cell Biol 4, E236–E242.

Almeida CG, Yamada A, Tenza D, Louvard D, Raposo G, Coudrier E (2011). Myosin 1b promotes the formation of post-Golgi carriers by regulating actin assembly and membrane remodeling at the *trans*-Golgi network. Nat Cell Biol 13, 779–789.

Andres-Delgado L, Anton OM, Madrid R, Byrne JA, Alonso MA (2010). Formin INF2 regulates MAL-mediated transport of Lck to the plasma membrane of human T lymphocytes. Blood 116, 5919–5929.
Bartolini F, Gundersen GG (2010). Formins and microtubules. Biochim Biophys Acta 1803, 164–173.
Bartolini F, Moseley JB, Schmoranzer J, Cassimeris L, Goode BL, Gundersen GG (2008). The formin mDia2 stabilizes microtubules independently of its actin nucleation activity. J Cell Biol 181, 523–536.
Beck KA, Buchanan JA, Nelson WJ (1997). Golgi membrane skeleton: identification, localization and oligomerization of a 195 kDa ankyrin isoform associated with the Golgi complex. J Cell Sci 110, 1239–1249.
Beck KA, Nelson WJ (1998). A spectrin membrane skeleton of the Golgi complex. Biochim Biophys Acta 1404, 153–160.
Boyer O *et al.* (2011). Mutations in INF2 are a major cause of autosomal dominant focal segmental glomerulosclerosis. J Am Soc Nephrol 22, 239–245.
Brown EJ, Schlondorff JS, Becker DJ, Tsukaguchi H, Uscinski AL, Higgs HN, Henderson JM, Pollak MR (2010). Mutations in the formin gene INF2 cause focal segmental glomerulosclerosis. Nat Genet 42, 72–U91.
Campellone KG, Webb NJ, Znameroski EA, Welch MD (2008). WHAMM is an Arp2/3 complex activator that binds microtubules and functions in ER to Golgi transport. Cell 134, 148–161.
Campellone KG, Welch MD (2010). A nucleator arms race: cellular control of actin assembly. Nat Rev Mol Cell Biol 11, 237–251.
Chen JL, Lacomis L, Erdjument-Bromage H, Tempst P, Stamnes M (2004). Cytosol-derived proteins are sufficient for Arp2/3 recruitment and ARF/coatomer-dependent actin polymerization on Golgi membranes. FEBS Lett 566, 281–286.
Chesarone MA, DuPage AG, Goode BL (2010). Unleashing formins to remodel the actin and microtubule cytoskeletons. Nat Rev Mol Cell Biol 11, 62–74.
Chhabra ES, Higgs HN (2006). INF2 is a WASP homology 2 motif-containing formin that severs actin filaments and accelerates both polymerization and depolymerization. J Biol Chem 281, 26754–26767.
Chhabra ES, Ramabhadran V, Gerber SA, Higgs HN (2009). INF2 is an endoplasmic reticulum-associated formin protein. J Cell Sci 122, 1430–1440.
Cole NB, Sciaky N, Marotta A, Song J, Lippincott-Schwartz J (1996). Golgi dispersal during microtubule disruption: regeneration of Golgi stacks at peripheral endoplasmic reticulum exit sites. Mol Biol Cell 7, 631–650.
Colon-Franco JM, Gomez TS, Billadeau DD (2011). Dynamic remodeling of the actin cytoskeleton by FMNL1 gamma is required for structural maintenance of the Golgi complex. J Cell Sci 124, 3118–3126.
de Marco MC, Martin-Belmonte F, Kremer L, Albar JP, Correas I, Vaerman JP, Marazuela M, Byrne JA, Alonso MA (2002). MAL2, a novel raft protein of the MAL family, is an essential component of the machinery for transcytosis in hepatoma HepG2 cells. J Cell Biol 159, 37–44.
Devarajan P, Stabach PR, Mann AS, Ardito T, Kashgarian M, Morrow JS (1996). Identification of a small cytoplasmic ankyrin (Ank(G119)) in the kidney and muscle that binds beta I sigma spectrin and associates with the Golgi apparatus. J Cell Biol 133, 819–830.
Dippold HC *et al.* (2009). GOLPH3 bridges phosphatidylinositol-4-phosphate and actomyosin to stretch and shape the Golgi to promote budding. Cell 139, 337–351.
Dubois T, Paleotti O, Mironov AA, Fraisier V, Stradal TEB, De Matteis MA, Franco M, Chavrier P (2005). Golgi-localized GAP for Cdc42 functions downstream of ARF1 to control Arp2/3 complex and F-actin dynamics. Nat Cell Biol 7, 353–U359.
Faul C, Asanuma K, Yanagida-Asanuma E, Kim K, Mundel P (2007). Actin up: regulation of podocyte structure and function by components of the actin cytoskeleton. Trends Cell Biol 17, 428–437.
Fucini RV, Sharma C, Stamnes MA (2000). Regulation of the actin cytoskeleton during vesicle formation on the Golgi apparatus. Mol Biol Cell 11, 1459.
Gaillard J, Ramabhadran V, Neumann E, Gurel P, Blanchoin L, Vantard M, Higgs HN (2011). Differential interactions of the formins INF2, mDia1, and mDia2 with microtubules. Mol Biol Cell 22, 4575–4587.
Gbadegesin RA *et al.* (2011). Inverted formin 2 mutations with variable expression in patients with sporadic and hereditary focal and segmental glomerulosclerosis. Kidney Int. doi: 10.1038/ki.2011.297.
Guzik-Lendrum S, Nagy A, Takagi Y, Houdusse A, Sellers JR (2011). *Drosophila melanogaster* myosin-18 represents a highly divergent motor with actin tethering properties. J Biol Chem 286, 2421755–21766.
Higgs HN (2005). Formin proteins: a domain-based approach. Trends Biochem Sci 30, 342–353.
Higgs HN, Peterson KJ (2005). Phylogenetic analysis of the formin homology 2 (FH2) domain. Mol Biol Cell 16, 1–13.
Holleran EA, Holzbaur ELF (1998). Speculating about spectrin: new insights into the Golgi-associated cytoskeleton. Trends Cell Biol 8, 26–29.
Kondylis V, Pannerden H, Herpers B, Friggi-Grelin F, Rabouille C (2007). The Golgi comprises a paired stack that is separated at G2 by modulation of the actin cytoskeleton through Abi and Scar/WAVE. Dev Cell 12, 901–915.
Kovar DR (2006). Molecular details of formin-mediated actin assembly. Curr Opin Cell Biol 18, 11–17.
Kovar DR, Pollard TD (2004). Progressing actin: formin as a processive elongation machine. Nat Cell Biol 6, 1158–1159.
Lee HK, Han KH, Jung YH, Kang HG, Moon KC, Ha IS, Choi Y, Cheong HI (2011). Variable renal phenotype in a family with an INF2 mutation. Pediatric Nephrol 26, 73–76.
Lenart P, Bacher CP, Daigle N, Hand AR, Eils R, Terasaki M, Ellenberg J (2005). A contractile nuclear actin network drives chromosome congression in oocytes. Nature 436, 812–818.
Li HB, Guo FL, Rubinstein B, Li R (2008). Actin-driven chromosomal motility leads to symmetry breaking in mammalian meiotic oocytes. Nat Cell Biol 10, 1301–U1101.
Liao GN, Ma XH, Liu G (2011). An RNA-zipcode-independent mechanism that localizes Dia1 mRNA to the perinuclear ER through interactions between Dia1 nascent peptide and Rho-GTP. J Cell Sci 124, 589–599.
Lippincott-Schwartz J, Zaal KJ (2000). Cell cycle maintenance and biogenesis of the Golgi complex. Histochem Cell Biol 114, 93–103.
Madrid R *et al.* (2010). The formin INF2 regulates basolateral-to-apical transcytosis and lumen formation in association with Cdc42 and MAL2. Dev Cell 18, 814–827.
Millan J, Puertollano R, Fan L, Rancano C, Alonso MA (1997). The MAL proteolipid is a component of the detergent-insoluble membrane subdomains of human T-lymphocytes. Biochem J 321, 247–252.
Miserey-Lenkei S, Chalancon G, Bardin S, Formstecher E, Goud B, Echard A (2010). Rab and actomyosin-dependent fission of transport vesicles at the Golgi complex. Nat Cell Biol 12, 645–654.
Puertollano R, Alonso MA (1999). MAL, an integral element of the apical sorting machinery, is an itinerant protein that cycles between the *trans*-Golgi network and the plasma membrane. Mol Biol Cell 10, 3435–3447.
Schuh M, Ellenberg J (2008). A new model for asymmetric spindle positioning in mouse oocytes. Curr Biol 18, 1986–1992.
Sun H, Schlondorff JS, Brown EJ, Higgs HN, Pollak MR (2011). Rho activation of mDia formins is modulated by an interaction with inverted formin 2 (INF2). Proc Natl Acad Sci USA 108, 2933–2938.
von Blume J, Alleaume A-M, Cantero-Recasens G, Curwin A, Carreras-Sureda A, Zimmermann T, van Galen J, Wakana Y, Valverde MA, Malhotra V (2011). ADF/cofilin regulates secretory cargo sorting at the TGN via the Ca(2+) ATPase SPCA1. Dev Cell 20, 652–662.
von Blume J, Duran JM, Forlanelli E, Alleaume AM, Egorov M, Polishchuk R, Molina H, Malhotra V (2009). Actin remodeling by ADF/cofilin is required for cargo sorting at the *trans*-Golgi network. J Cell Biol 187, 1055–1069.
Wozniak MJ, Bola B, Brownhill K, Yang YC, Levakova V, Allan VJ (2009). Role of kinesin-1 and cytoplasmic dynein in endoplasmic reticulum movement in VERO cells. J Cell Sci 122, 1979–1989.
Zilberman Y, Alieva NO, Miserey-Lenkei S, Lichtenstein A, Kam Z, Sabanay H, Bershadsky A (2011). Involvement of the Rho-mDia1 pathway in the regulation of Golgi complex architecture and dynamics. Mol Biol Cell 22, 2900–2911.